

Article

Highly Effective Pt-Co/ZSM-5 Catalysts with Low Pt Loading for Preferential CO Oxidation in H₂-Rich Mixture

Marina Shilina ^{1,*}, Irina Krotova ¹, Sergey Nikolaev ¹, Sergey Gurevich ², Denis Yavsin ² , Olga Udalova ³ and Tatiana Rostovshchikova ¹

¹ Department of Chemistry, Lomonosov Moscow State University, 119991 Moscow, Russia

² Ioffe Physico-Technical Institute, RAS, 194021 St. Petersburg, Russia

³ Semenov Federal Research Center for Chemical Physics, RAS, 119991 Moscow, Russia

* Correspondence: mish@kinet.chem.msu.ru

Abstract: New Pt-Co catalysts of hydrogen purification from CO impurities for fuel cells were fabricated via the deposition of monodispersed 1.7 nm Pt nanoparticles using laser electrodispersion on Co-modified ZSM-5 prepared by the Co(CH₃COO)₂ impregnation. The structure of prepared Pt-Co zeolites was studied by low-temperature N₂ sorption, TEM, EDX, and XPS methods. The comparative analysis of samples with different Pt (0.01–0.05 wt.%) and Co (2.5–4.5 wt.%) contents on zeolites with the ratio of Si/Al = 15, 28, and 40 was performed in the CO-PROX reaction in H₂-rich mixture (1%CO + 1%O₂ + 49%H₂ + 49%He). The synergistic catalytic action of Pt and Co on zeolite surface makes it possible to completely remove CO from a mixture with hydrogen in a wide temperature range from 50 to 150 °C; the high efficiency of designed composites with low Pt loading is maintained for a long time. The enhancement of PROX performance originates from the formation of new active sites for the CO oxidation at the Pt-Co interfaces within zeolite channels and at the surface. In terms of their activity, stability, and selectivity, such composites are significantly superior to known supported Pt-Co catalysts.



Citation: Shilina, M.; Krotova, I.; Nikolaev, S.; Gurevich, S.; Yavsin, D.; Udalova, O.; Rostovshchikova, T. Highly Effective Pt-Co/ZSM-5 Catalysts with Low Pt Loading for Preferential CO Oxidation in H₂-Rich Mixture. *Hydrogen* **2023**, *4*, 154–173. <https://doi.org/10.3390/hydrogen4010011>

Academic Editors: Aleksey A. Vedyagin and Ekaterina V. Shelepova

Received: 16 January 2023

Revised: 2 February 2023

Accepted: 14 February 2023

Published: 16 February 2023



Copyright: © 2023 by the authors. Licensee MDPI, Basel, Switzerland. This article is an open access article distributed under the terms and conditions of the Creative Commons Attribution (CC BY) license (<https://creativecommons.org/licenses/by/4.0/>).

Keywords: hydrogen purification technologies; CO-PROX; platinum; laser electrodispersion; cobalt; zeolite; catalysis

1. Introduction

The most promising technologies to obtain energy are based on proton exchange membrane fuel cells (PEMFC), which are clean and sustainable energy sources [1]. Pure hydrogen is the ideal fuel for the PEMFC. High concentrations of CO can be removed from the reformat streams by the water–gas shift reaction (WGS), during which it reacts with water to yield CO₂ and H₂. However, the residual concentration of CO is too high to feed the PEMFCs. Even traces of CO in the hydrogen-rich feed gas poison the platinum anode electrode and dramatically decrease the power output. The preferential CO oxidation (CO-PROX) in H₂-rich mixture is a necessary step in the purification of hydrogen-rich reformates in order to use them as feeds for PEMFCs. It allows reaching tolerable CO values for the fuel cell (below 10 ppm) [2–7]. PEMFCs usually operate in the temperature range of 60–80 °C, and conversion of CO to CO₂ without oxidation of H₂ should proceed at these working temperatures. This should reduce the number of cooling stages, eliminate losses due to undesirable H₂ oxidation, and optimize the path from production to use of hydrogen.

Furthermore, the key factors in the design of CO-PROX catalysts are high activity at moderately low temperatures and a wide range of their selective and stable operations. Two main types of PROX catalysts with high activity for carbon monoxide removal and relatively lower hydrogen consumption have been reported in the literature. They include noble metal catalysts; among them, platinum is the most promising one [8]. Only platinum catalyst made it possible to completely remove CO from the mixture with H₂, under the

same conditions Pd- and Ru-supported catalysts turned out to be inefficient [9]. The easy formation of the hydride phase increases the Pd catalyst activity in the H₂ oxidation, and accordingly, reduces the selectivity of CO oxidation [10]. The other group of catalysts is based on transition metals, such as Co, Ni, Cu, and their oxides [11–13]. In terms of their activity in CO oxidation, catalysts based on cobalt oxides are only slightly inferior to noble metal ones [14]. For example, mixed oxides of cobalt with cerium are successfully used in CO-PROX [15,16]. However, they are often inferior to platinum-based catalysts in their selectivity and stability. Carbonate formation in the presence of CO₂ and water may be responsible for their deactivation. Recent studies have shown that Co- and Co/Ce-modified zeolites obtained by impregnation are active in the CO oxidation in both in the absence and presence of hydrogen [17–19].

The Pt catalysts exhibit high activity and selectivity, while improvement on its low temperature activity is needed. However, the high CO adsorption of Pt catalysts blocking its active sites toward the O₂ adsorption leads to the fact that 100% CO conversion on Pt/Al₂O₃ catalysts is achieved only at elevated temperatures of 170–200 °C, when hydrogen oxidation starts. Therefore, the selectivity of unmodified Pt catalysts is not very high [20,21]. Another significant disadvantage of Pt catalysts is their high cost. Many attempts are being made to reduce the platinum content in catalysts. Design of low loaded but highly efficient Pt catalysts for the CO oxidation requires the use of precise methods to produce finely dispersed catalysts with a special local structure of platinum [22–27]. Single atom catalysts that allow the most efficient use of noble metals are attracting attention as an alternative to supported catalysts based on metal nanoparticles [4,28,29]. However, there is a problem of a low stability for highly dispersed systems.

Recently, the interest in PROX catalysts has concentrated on Pt-based bimetallic catalysts, which show much better activity, selectivity, and stability than monometallic ones. Different metals and promoters, such as Ru, Ni, Sn, Fe, Ce, Co, and others, have been tested for their ability to increase catalytic activity in PROX [30–36]. Among the promoters, Co is the most common additive in Pt-supported catalysts as it shows good performance with PROX, but most often a high Pt content (about 1% or more) is required [37–41]. The important problem to design high-performance PROX catalysts with a reduced noble metal content remains unresolved. To solve it, it is necessary to take into account the main factors that control the structure and properties of the catalytic system, and accordingly, the mechanism of the catalytic action. Although CO oxidation is one of the most studied catalytic processes [42], the nature of active states, especially in bimetallic supported catalysts (metallic states or cations and oxides, alloyed particles or solid solutions), is still under discussion [38–41,43–46]. The high performance of both (alloyed and not alloyed) Pt-Co bimetallic systems exhibits the key role of Pt-Co interface.

Support type and synthesis method play a key role in achieving the high degree of interaction of active components [47–49]. Many studies have indicated that the use of zeolites as supports for platinum catalysts is promising to improve the catalyst activity, selectivity and stability for the oxidation of CO and some other pollutants [7,9,50–59]. The role of metal-support interactions increases with a decrease in the metal content. Therefore, the problem of the formation of uniform centers on the catalyst surface becomes much more complicated, especially in the case of bimetallic systems. Special synthesis methods, such as inorganic colloidal synthesis [22,60], are useful to control particle size and composition. Recently, physical methods based on laser ablation are considered to be a more controlled and environmentally friendly alternative to chemical synthesis [61]. Among them, the method of laser electrodispersion (LED) has been successfully used for the fabrication of highly active “crust-like” catalysts [62,63]. The selective deposition of one-size nanoparticles only on the outer support surface makes the active phase available for reagents and for structural studies. Low loaded Pt and Pd catalysts were unusually active in the CO oxidation in an inert atmosphere compared to counterparts prepared by standard chemical synthesis [64–66]. In activity, Pd-modified HZSM-5 zeolites outperformed samples on aluminum oxide with the same particle size also prepared via LED. The best activity of

catalysts on zeolite originates from the optimal electronic state of metal containing metallic and oxidized states favorable for oxidation.

In this work, we combine the advantages of two methods of introducing active Pt and Co components into the zeolite to design high-performance CO-PROX catalysts with a low Pt loading. For this purpose, we applied the original method of laser electrodispersion for selective deposition of small amounts of finely dispersed Pt on Co/ZSM-5 pre-modified by the $\text{Co}(\text{CH}_3\text{COO})_2$ impregnation. The use of zeolites with different Si/Al ratio allows for the stabilization of Co in the form of oxo-cations that are more active in the CO oxidation compared with Co_3O_4 and CoO , and additionally, to achieve the close Pt-Co contacts. New active sites at the Pt-Co interfaces make it possible to reduce the CO concentration in H_2 -rich gas streams below 10 ppm at relatively low temperatures.

2. Materials and Methods

2.1. Catalyst Preparation

Zeolites $\text{NH}_4\text{ZSM-5}$ ("Zeolyst", Si/Al = 15, 28, 40) were used to obtain the HZSM-5 (HZ) by calcination at $550\text{ }^\circ\text{C}$ in an air stream for 8 h. Cobalt modified zeolites (Co/Z) were synthesized in accordance with [17,18] by the incipient wetness impregnation of dried HZSM-5, with the aqueous solution of desired amount of $\text{Co}(\text{CH}_3\text{COO})_2 \cdot 4\text{H}_2\text{O}$ then dried for 1 day at room temperature and for 8 h at $120\text{ }^\circ\text{C}$. Finally, they were calcined at $450\text{ }^\circ\text{C}$ for 3 h in flowing air. The Co content in zeolites was 2.5 or 4.5 wt.%.

Monodispersed Pt nanoparticles were deposited on HZ or Co/Z using laser electrodispersion (LED) technique, described in detail in [62,63]. The deposition time was chosen based on the rate of Pt deposition determined previously [65]. It was 110 or 550 s to load 0.01 or 0.05 wt.% Pt on 1g of zeolite. In some cases, the order was reversed—first platinum was deposited by LED, and then cobalt was introduced by impregnation. Depending on the synthesis procedure, the samples were designated as Pt/Co/Z or Co/Pt/Z. The schematic diagram of the typical synthesis of Pt/Co/Z catalysts is shown in Figure 1. The catalysts were stored in air and activated before catalytic tests by heating for 1 h at $350\text{ }^\circ\text{C}$ in He. All prepared catalysts are listed in Table 1.

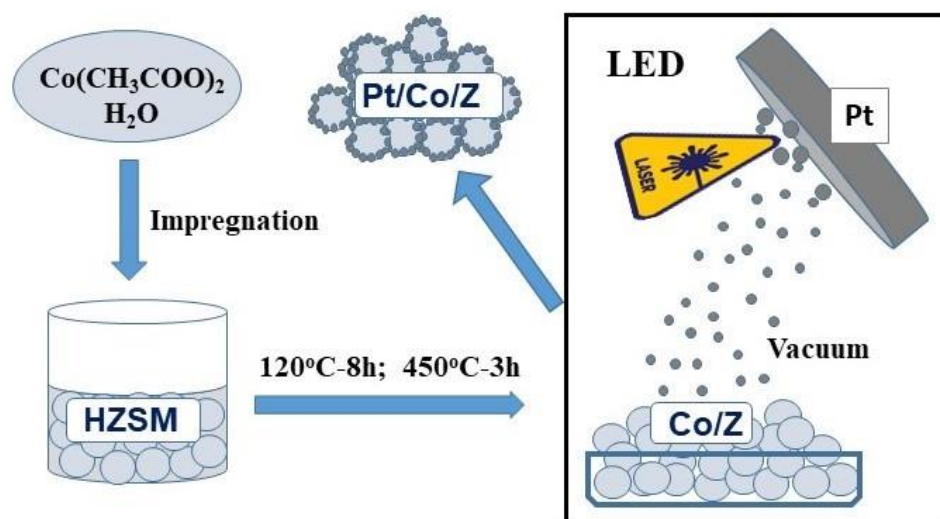


Figure 1. Schematic diagram of the catalyst preparation for the example of Pt/Co/Z.

2.2. Catalyst Characterization

Thermo iCE 3000 spectrometer (Thermo FisherScientific Inc., Intertech Corporation, Waltham, MA, USA) was used to analyze Pt and Co contents in the catalysts. The results of AAS measurements agreed with the calculated values given in Table 1.

Table 1. Pt- and Co-modified HZSM-5 zeolites.

Sample	Si/Al	Pt, wt. %	Co, wt. %	Co/Al ¹
0.01Pt/Z-15	15	0.01	-	-
0.05Pt/Z-15	15	0.05	-	-
0.01Pt /Z-28	28	0.01	-	-
0.05Pt /Z-28	28	0.05	-	-
4.5Co/Z-15	15	-	4.5	0.75
4.5Co/Z-28	28	-	4.5	1.4
2.5Co/0.01Pt/Z-15	15	0.01	2.5	0.42
0.01Pt/2.5Co/Z-15	15	0.01	2.5	0.42
0.01Pt/4.5Co/Z-15	15	0.01	4.5	0.75
0.05Pt/4.5Co/Z-15	15	0.05	4.5	0.75
0.01Pt/2.5Co/Z-28	28	0.01	2.5	0.75
4.5Co/0.01Pt/Z-28	28	0.01	4.5	1.4
0.01 Pt/4.5Co/Z-28	28	0.01	4.5	1.4
0.05Pt/2.5Co/Z-28	28	0.05	2.5	0.75
0.01Pt/2,5Co/Z-40	40	0.01	2.5	1.1
0.01Pt/4.5Co/Z-40	40	0.01	4.5	1.8

¹ Co/Al, calculated as Co to framework aluminum AlF atomic ratio.

The SEM analysis of the catalyst surfaces was carried out on a JSM-6000 NeoScope scanning electron microscope (JEOL, Akishima, Japan) with an EX-230 energy dispersive X-ray analyzer. Images were recorded in a high vacuum mode with an accelerating voltage of 10–15 kV. Secondary electron image (SEI) detection was used.

The samples were studied by transmission electron microscopy (TEM) on a JEOL JEM 2100F/UHR instrument (JEOL Ltd., Tokyo, Japan) integrated with a JEOL JED-2300 Analysis Station Plus EDX system. Sample preparation for TEM studies was described in detail [64]. The average particle size was determined from the particle size distribution histograms. Data for a total of 300 particles were processed statistically. Lattice spacing (d) was determined using the ImageJ 1.47 program (<https://imagej.nih.gov/char188/download.html>, accessed on 10 July 2021). The crystal structures of the ordered atomic domains were identified using the ICDD data base (<https://www.icdd.com> (PDF-2) accessed on 10 July 2021).

The texture characteristics of the zeolites were determined after heating in vacuum at 350 °C; for 3 h by low-temperature nitrogen adsorption using an Autosorb-1 sorption analyzer (Quantachrome, Boynton Beach, FL, USA). The specific surface area was calculated by the BET and V-t methods, while the total pore volume was determined at P/P₀ = 0.995.

X-ray photoelectron spectroscopy (XPS) study was performed on an Axis Ultra DLD spectrometer (Kratos Analytical Limited, Manchester, UK) with a monochromatic Al K α source (h ν = 1486.7 eV, 150 W) at a transmission energy of 160 and 40 eV. To reduce the effect of sample charging, the energy scale of the XPS spectra was preliminarily calibrated using the characteristic Si 2p peak at 103.6 eV.

Powder X-ray diffraction patterns were collected within the 10 to 40 2 θ range on a DRON-3M diffractometer with Cu K α radiation.

The infrared spectra (FTIR) of the samples were obtained on an Infracum FT-801 (Lyumeks-Sibir, Russia) Fourier spectrometer with a resolution of 2 cm⁻¹ in the spectral range of 450–2000 cm⁻¹ in the KBr phase.

2.3. Catalytic Tests

The catalytic oxidation was performed at 50–250 °C with the initial gas mixture CO:O₂:H₂:He=1:1:49:49 (v/v) in a fixed-bed quartz reactor in the flow regime, as was described [19]. Heating-cooling cycles were carried out, temperature was changed in steps of 20 °C, and each temperature was maintained for 20 min. Catalyst (250 mg of 40–60 mesh fraction) mixed with an equivalent amount of quartz sand was used. The composition of the gas mixture at the reactor outlet was analyzed using a Crystal 2000 chromatograph

(Chromatec SDO JSC, Russia) equipped with a thermal conductivity detector (flow rate $10 \text{ cm}^3 \text{ min}^{-1}$). Methane was not found in the reaction products.

The CO conversion was found from the formula

$$X_{\text{CO}} = \frac{[\text{CO}]_{\text{in}} - [\text{CO}]_{\text{out}}}{[\text{CO}]_{\text{in}}} \cdot 100\%,$$

where $[\text{CO}]_{\text{in}}$ and $[\text{CO}]_{\text{out}}$ are the concentrations of CO (vol. %) at the reactor inlet and outlet, respectively. The catalytic activity was assessed from the temperature dependences of the CO conversion, the temperatures corresponding to 50% and maximum conversion of CO (T_{50} and T_{max} , respectively) and operating window ΔT_{100} of the 100% conversion of CO were used.

3. Results and Discussion

3.1. The Structure of Catalysts

3.1.1. Catalysts Morphology

The structure of the zeolite is preserved when modified with Co and Pt using methods of impregnation and LED, respectively. It is confirmed by the presence of XRD reflexes corresponding to ZSM-5 (Figure S1). The absence of reflexes corresponding to crystalline Co metal and the oxide phases of CoO or Co_3O_4 indicates that samples of ZSM-5 zeolite modified with 2.5–4.5% Co contain mainly ionic or highly dispersed cobalt species [17,67].

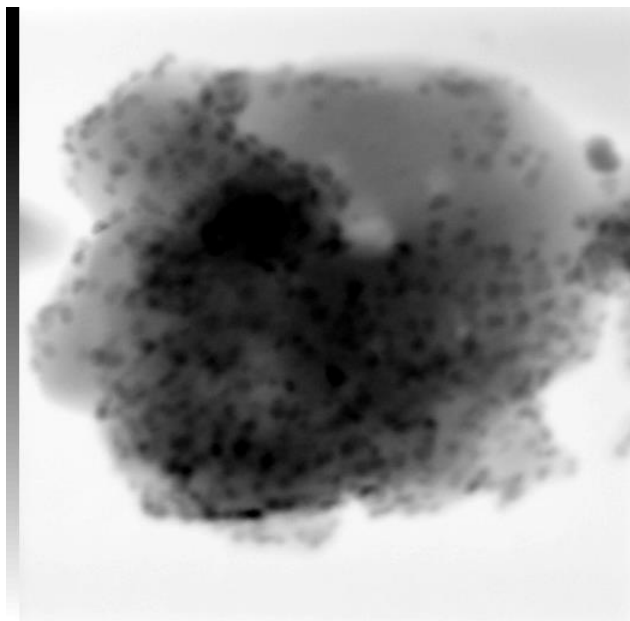
Pt nanoparticles formed by the LED method have a size of 1.7–1.9 nm, regardless of the metal loading and the support type, as was previously shown [62,65]. They remain in the form of single particles even in dense coatings. High resistance to aggregation is an important common feature of amorphous nanoparticles formed by the LED method from liquid metal droplets [62–66]. Co-modified zeolite Co/ZSM-5 may contain three types of Co species depending on the Co/Al ratio: bare Co^{2+} cations or oxo-cations $[\text{Co}_x\text{O}_y]^{n+}$ with $n = 1, 2$ within zeolite channels and cobalt oxides on the outer zeolite surface [17–19]. Only small spherical Co species of 2 nm in size with a regular surface distribution are predominant in the zeolites prepared by impregnation when $\text{Co}/\text{Al} < 1$. In accordance with [17,18,67] such type of particles was associated with the Co counter ions or oxo-cations originally located in zeolite channels. Exposure to high-energy TEM beam leads to the migration of Co to the surface of the zeolite grains and sintering of cobalt particles of about 2 nm. When $\text{Co}/\text{Al} > 1$, the slightly larger particles with distinct crystal faces of cobalt oxides can be seen in HRTEM images at the edges of zeolites.

Typical images of monometallic Pt- and Co-modified zeolites are shown in Figures S2 and S3. They also indicate that ZSM-5 structure is preserved during the Pt deposition. Only highly dispersed spherical particles are clearly visible in the Pt images (Figure S3a,b). For some locations of ordered atoms in Pt particle images, the lattice spacing of 2.7 Å was found, which is close to the value for the PtO (111) face ($d = 2.67 \text{ Å}$, <https://materialsproject.org>, DOI 10.17188/1188047). Two types of particles are present in the Co images: faintly distinguishable small particles and larger particles located predominantly at the edge of zeolite (Figure S3c,d). The lattice spacing for the regions of ordered Co atoms were 2.8 and 4.9 Å, which are close to that in the Co_3O_4 (220) and (111) faces (JCPDS 80-1543, $d = 2.88$ and 4.77 Å).

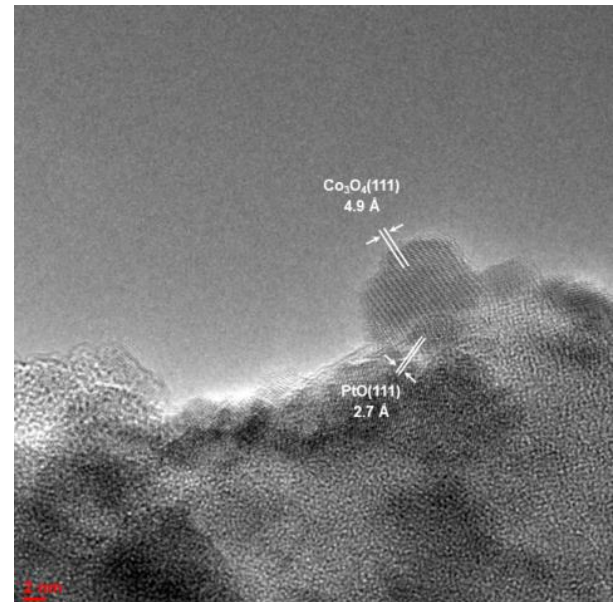
Figure 2 presents the typical TEM images of bimetallic Pt/Co/Z zeolite; other examples are given in Figures S4–S7. All images demonstrate highly dispersed dark species uniformly distributed on the gray surface of zeolite matrix. According to EDX data (Figures 2d,e, S4, S6 and S7b), they correspond to Pt- and Co-containing nanoparticles. The lattice spacing determined for some ordered atomic domains in the supported particles equal 2.3 and 2.7 Å (PtO), as well as 3.0 and 4.9 Å (Co_3O_4), which are associated with neighboring Pt and Co oxides. Typical histograms of the particle size distribution (Figure 2f and Figures S5b and S7c) are bimodal, and approximately half of the particles have a size of $1.7 \pm 0.3 \text{ nm}$, whereas the remaining particles have a wide size distribution with an average size of 7 nm. In accordance with previous data [17,62,63], highly dispersed particles can

be attributed to both Pt species and Co-cations or oxo-cations originally located in zeolite channels; the large particles most likely correspond to Co oxides closely located with Pt oxides (Figure 2b) or mixed Pt-Co oxides (Figure S5a) on the zeolite surface.

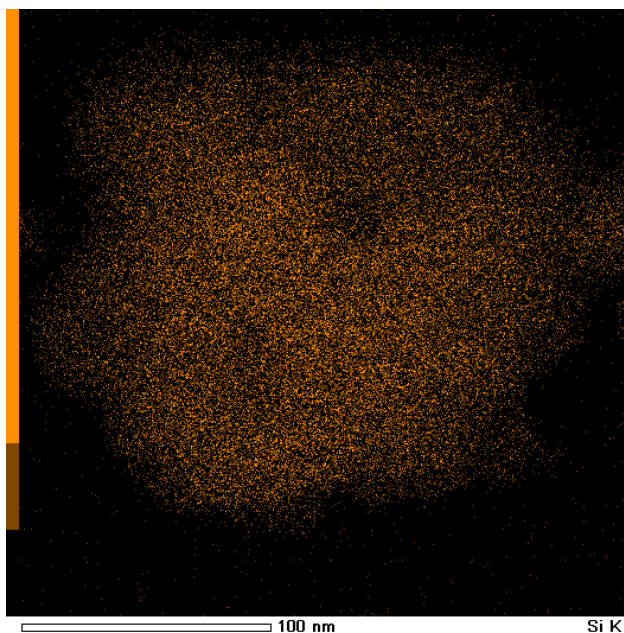
Typical SEM images of modified zeolites (Figure S8), as well as TEM ones, indicate that both Co and Pt species are uniformly distributed at the same locations on the zeolite surface.



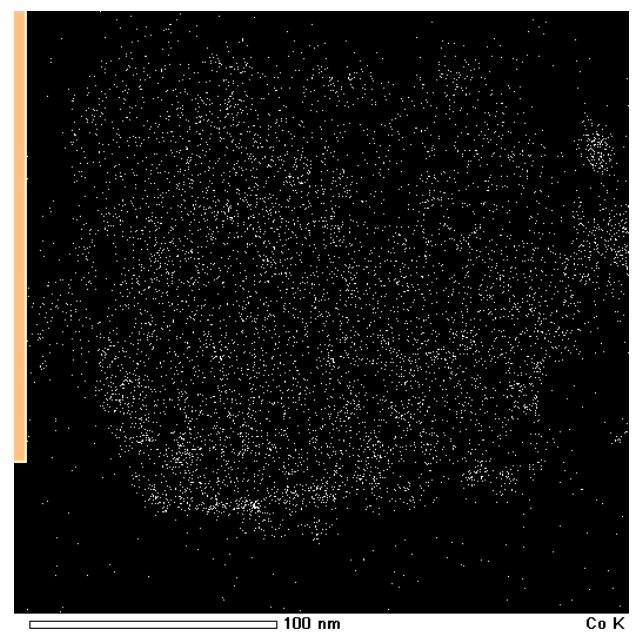
(a)



(b)



(c)



(d)

Figure 2. Cont.

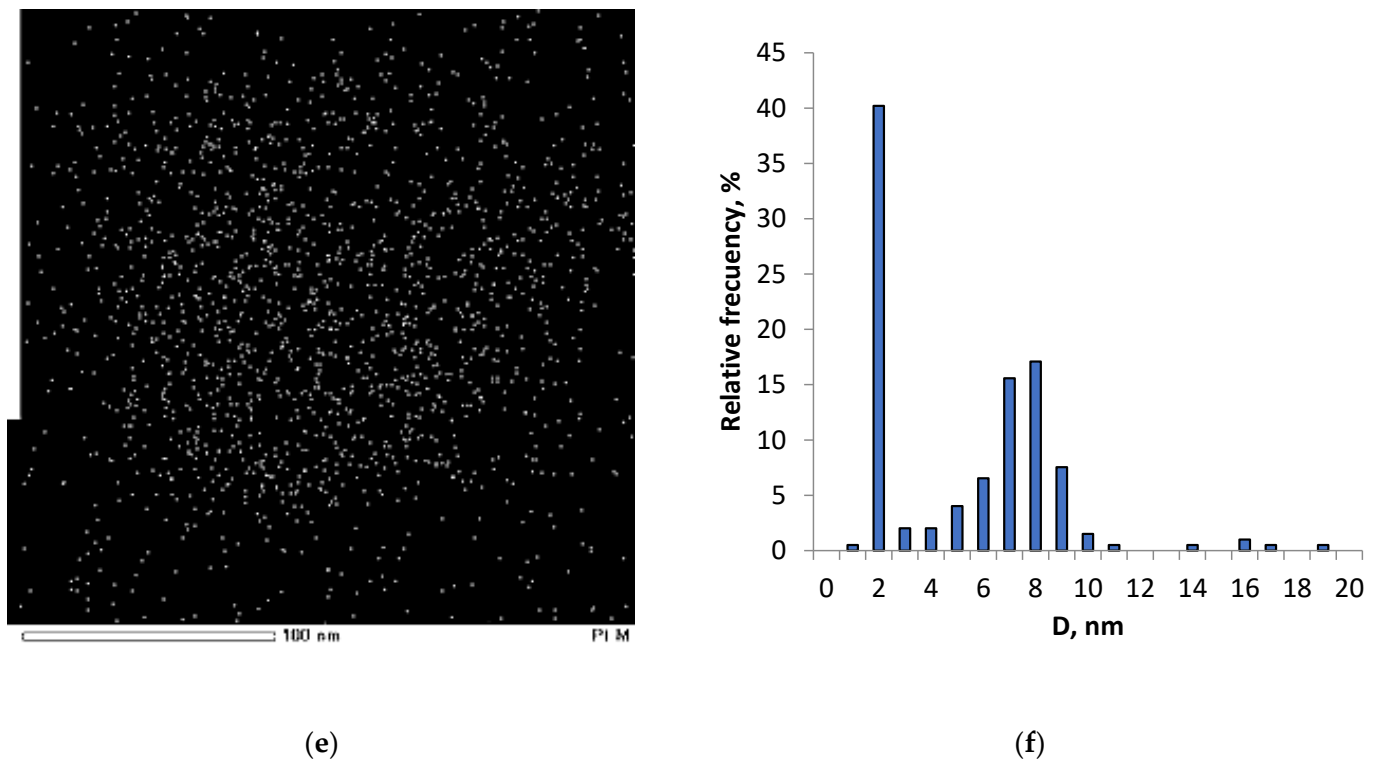


Figure 2. (a,b) TEM images; (c) Si, (d) Co, and (e) Pt EDX element distribution maps; and (f) particle size distribution of the 0.05Pt/2.5Co/Z-28 sample.

The textural characteristics of parent and Pt- and Co-modified zeolites are presented in Table 2. The Pt deposition changes the textural characteristics of all zeolites just a little. When a small amount of platinum (0.01%) is deposited on a more acidic Z-15 zeolite, platinum interacts with the acid sites of the support and partially penetrates into the channels of the zeolite. This slightly reduces the specific surface, especially the values of $S_{\text{micropore}}$ and V_{pore} . The deposition of a larger amount of highly dispersed platinum particles mainly on the outer surface of a less acidic zeolite leads to a slight increase in the surface size of 0.05Pt/Z-28. In contrast, the introduction of cobalt via an impregnation noticeably reduces the surface area and pore volume of the zeolite. This reduction is more pronounced for the zeolite with the lowest Si/Al ratio of 15. This is consistent with previous adsorption and spectral studies of Co-modified zeolites [17–19]. When Co/Al < 1 (see Table 1), a significant Co part is located inside the channels of the zeolite. In this case textural characteristics of bimetallic Pt-Co samples are close to those of cobalt-modified zeolites.

Table 2. The textural properties of parent and Pt- and Co-modified zeolites.

Sample	$S_{\text{BET}}, \text{m}^2/\text{g}$	$S_{\text{V-tr}}, \text{m}^2/\text{g}$		$V_{\text{pore}}, \text{cm}^3/\text{g}$
		Micropore	External	
Z-15	444	425	19	0.18
4.5Co/Z-15	389	368	21	0.15
0.01Pt/Z-15	428	408	20	0.17
0.01Pt/4.5Co/Z-15	350	320	30	0.14
0.05Pt/4.5Co/Z-15	388	370	18	0.15
Z-28	462	446	16	0.18
2.5Co/Z-28	436	419	17	0.15
4.5Co/Z-28	425	406	19	0.15
0.05Pt/Z-28	490	474	16	0.19
0.05Pt/2.5Co/Z-28	446	419	27	0.17

3.1.2. FTIR Spectroscopy Studies

Figure 3 shows the FTIR transmittance spectra of initial and Pt/Co-modified zeolites Z-28 and Z-30 in the ranges 450–2000 and 500–900 cm^{-1} . The bands near 1100–1200, 797, and 458 cm^{-1} are assigned to vibrations of TO_4 (T = Si or Al) tetrahedra; the bands at 620 and 550 cm^{-1} are characteristic of double-rings of tetrahedra in the framework [68]. As can be seen in Figure 3, the position of the bands at 550 and 797 cm^{-1} did not change in all samples, indicating that the structure of ZSM-5 did not alter after loading Co by impregnation and Pt by LED methods.

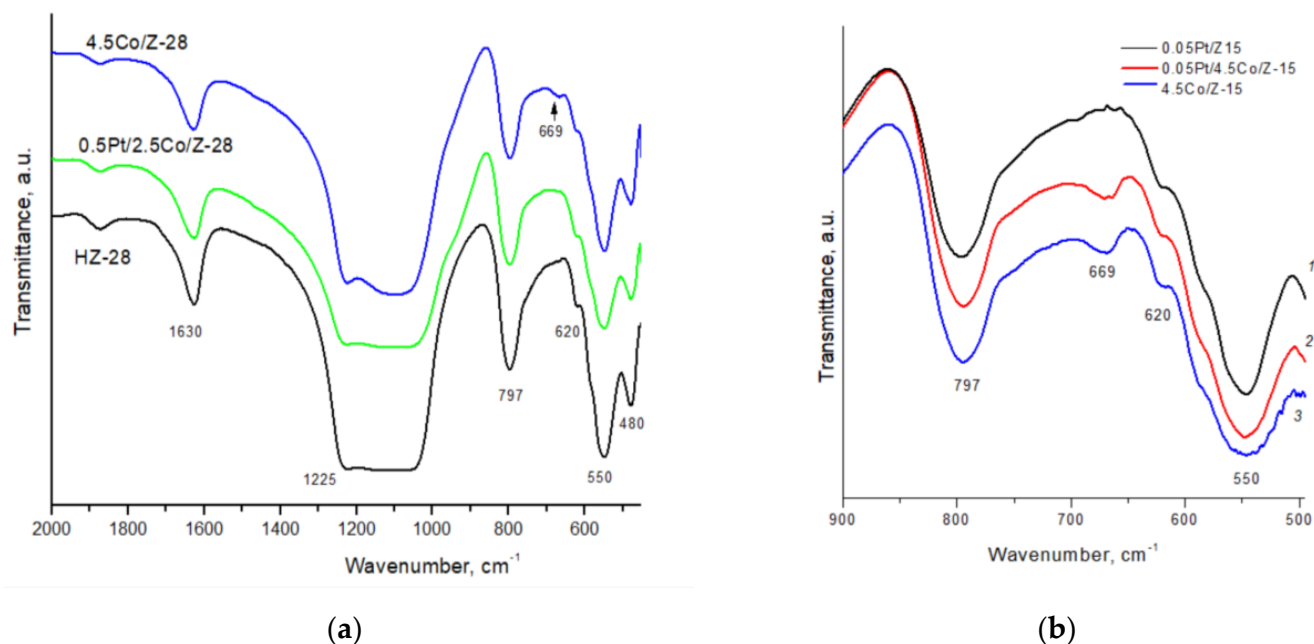


Figure 3. FTIR spectra of (a): HZ-28, 0.05Pt/2.5Co/Z-28, and 4.5Co/Z-28; (b): 0.05Pt/Z-15 (1), 0.05Pt/4.5Co/Z-15 (2), and 4.5Co/Z-15 (3) in KBr.

In the samples containing 4.5% Co a small band appears near 669 cm^{-1} due to stretching vibrations of the metal–oxygen bond in Co_3O_4 [69,70]. This band is attributed to the ABO_3 vibrations where B denotes the Co(III) in an octahedral position and A stands for the Co(II) in a tetrahedral holes [69]. The bands of the zeolite framework mask the second band associated with OB vibrations in the spinel lattice, located near 560 cm^{-1} . Small bands of Co_3O_4 are observed in IR spectra of both monometallic and bimetallic Pt/Co zeolites only at a loading of 4.5% Co, while for samples containing 2.5% Co, spinel oxide bands are not recorded. Thus, the obtained results show that only a small fraction of cobalt forms oxide structures on the surface. The main part of cobalt is located in the ionic form in the channels of the zeolite, and the crystal structure of the latter does not change with the introduction of modifying additives. This is consistent with the XRD and TEM data.

3.1.3. XPS Studies

The analysis of XPS spectra of Pt-modified zeolites with low Pt loading is a challenge due to overlapping of the Pt4f and Al2p lines. Earlier Pt/ Al_2O_3 catalysts with ultralow metal loadings of 0.02–0.005 wt.% also prepared by LED were successfully studied by XPS [65]. Along with the Al2p component, three Pt4f doublets with the spin-orbital splitting of 3.34 eV attributed to Pt^0 , Pt^{2+} , and Pt^{4+} species were used for the fitting of overlapped Pt4f–Al2p spectra. The doublet of asymmetrical lines was used for the Pt^0 components, and for the other components, doublets of symmetrical lines. The typical Pt4f spectra are shown in Figure 4a. with an example of the Pt- and Pt-Co-modified Z-28. The binding energies (BE) of the Pt4f_{7/2} components resulted from the spectra fitting along with those for Co2p_{3/2}, and Al2p are given in Table 3 for monometallic and bimetallic samples.

The Pt4f binding energies are close to those reported for Pt⁰ and oxidized Pt²⁺ and Pt⁴⁺ species or PtO and PtO₂ oxides [56,58,65]. In addition, the component with the medium binding energy between 72.4–72.6 eV can also be linked to partially positive Pt species (Pt^{δ+}: 0 < δ < 2) [24], and the component with the highest BE can be attributed not only to Pt⁴⁺ species but also to Pt²⁺ cations in the ion-exchange positions of HZSM-5 [71]. It may refer to the Ptⁿ⁺ (2 < n < 4) in the form of PtO_xAl strongly bound to the Al sites in zeolite that arises during the exchange of positively charged PtO_x particles with protons of the acid sites, as was shown for Pd-modified zeolites [64,72].

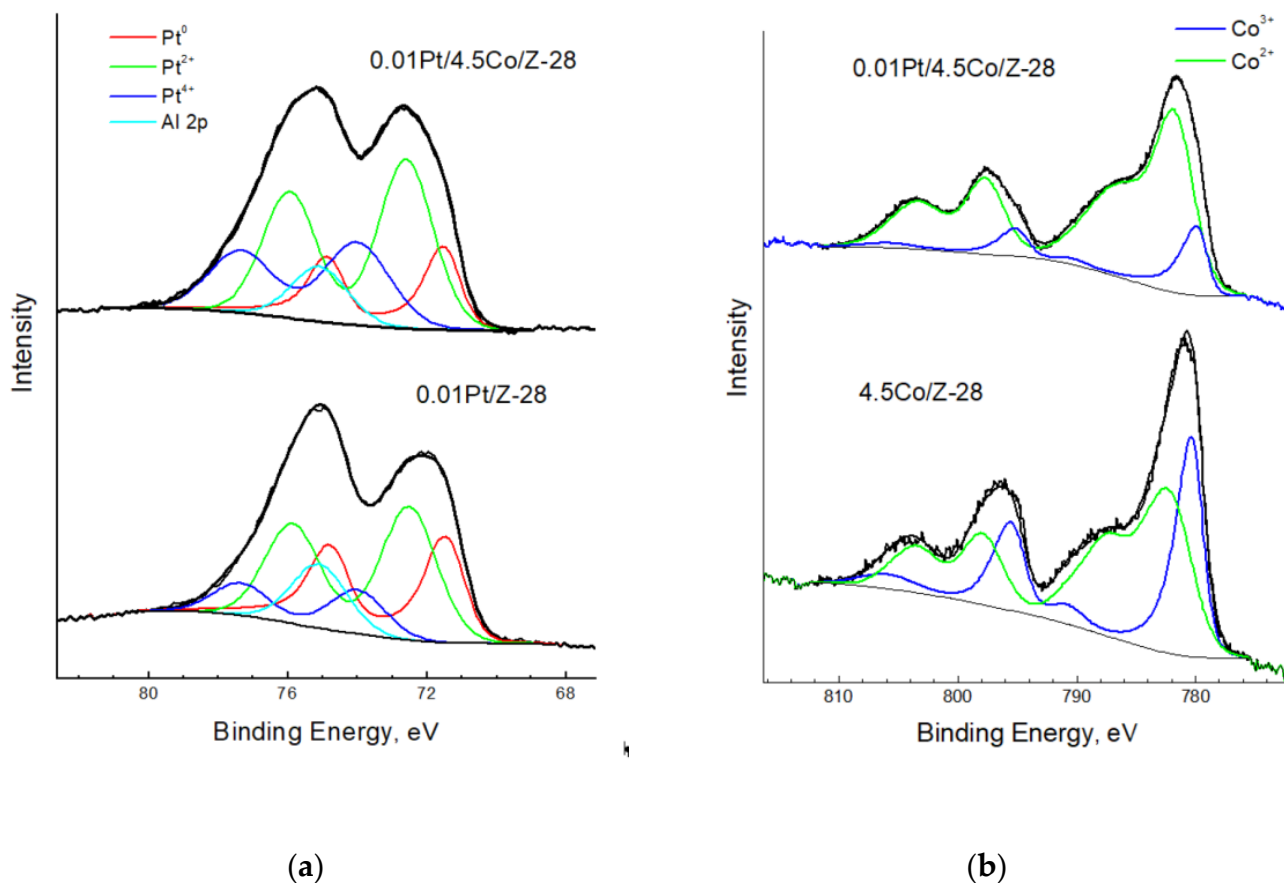


Figure 4. XP-spectra of (a) Pt4f and Al2p; (b) Co2p for 0.01Pt/4.5Co/Z-28; 0.01Pt/Z-28; and 4.5Co/Z-28.

Table 3. Binding energies (eV) of the XPS components in the spectra of Pt- and Co-modified zeolites (BE Si2p = 103.6eV).

Sample	Co2p _{3/2}		Pt4f _{7/2}		
	Co(III)	Co(II)	Pt ⁰	Pt ^{δ+} (PtO)	Pt ⁿ⁺ (PtO _x Al)
Pt/Z	–	–	71.4–71.6	72.4–72.6	74.0–74.5
Co/Z	779.8–780.4	782.0–782.6	–	–	–
Pt/Co/Z	780.0–780.4	781.9–783.0	71.6–71.7	72.6–72.7	74.2–74.7

The typical Co2p XP-spectra are presented in Figure 4b for Co- and Pt/Co Z-28. The broad Co 2p peaks have a similar shape and show a significant contribution from both divalent and trivalent cobalt. In addition to the main doublet of Co 2p_{3/2} and Co 2p_{1/2} lines at about 780–782 and 795–798 eV, the spectra exhibit intense “shake-up” satellites at higher binding energies, which are characteristic of Co(II) [73]. To analyze the fractions of Co(III) and Co(II) on the zeolite surface, Co 2p_{3/2} peaks and their satellites were decomposed as described in [17,18]. The corresponding binding energies for Co(III) and Co(II) components in monometallic and bimetallic zeolites are given in Table 3. The

relative shares of different Co and Pt states—and their total surface content derived from the decomposition of the XP-spectra of all samples studied—are given in Table 4.

Table 4. Percentages of different Pt and Co states and the relative surface content in Pt- and Co-modified zeolites (initial and spent in CO-PROX) determined by XPS.

Sample	Co, at. %			Pt/(Si + Al)	Pt, at. %		
	Co(III)	Co(II)	Co/(Si + Al)		Pt ⁰	Pt ^{δ+}	Pt ²⁺
0.01Pt/Z-15	-	-	-	0.05	36	21	43
0.01Pt/Z-28	-	-	-	0.11	35	49	16
0.05Pt/Z-28	-	-	-	0.22	61	24	15
4.5Co/Z-15	46	54	0.12	-	-	-	-
4.5Co/Z-28	39	61	0.17	-	-	-	-
0.01Pt/4.5Co/Z-15	initial	45	55	0.20	24	45	31
	spent	54	46	0.29	46	34	20
0.01 Pt/4.5Co/Z-28	16	84	0.09	0.10	20	50	30
4.5Co/0.01 Pt/Z-28	61	39	0.12	0.01	12	48	40
0.05Pt/2.5Co/Z-28	initial	47	53	0.11	57	20	23
	spent	75	25	0.32	0.24	77	8

As can be seen from the data in Table 4, Pt is present in all three states in monometallic and bimetallic samples. The presence of a significant amount of oxidized platinum on the zeolite surface is consistent with the results of TEM images (Figures 2b, S3 and S5), where the lattice spacing of 2.7 Å typical for PtO was found. The electronic state and relative Pt content on the surface are somewhat different. The Pt content on the surface increases not only with a growth in the loading of platinum from 0.01 to 0.05%, but also with the rise in the ratio of Si/Al in zeolite. The reduced content of platinum on the monometallic 0.01Pt sample with the lowest Si/Al = 15 indicates a possibility of the Pt interaction with the acid sites of zeolite, the number of which is maximized in this case. This probably leads to partial penetration of particles into the channels of the zeolite during the exchange of positively charged Pt species with protons of the acid sites. This is a rather unexpected result, since the main feature of the LED method is the selective deposition of metal nanoparticles on the outer surface of the support, as was observed for inert SiO₂ and Al₂O₃ oxides and carbon supports [62,63,65]. The maximum fraction of the Ptⁿ⁺ state with the highest BE in the most acidic zeolite confirms such interaction leading to the stabilization of highly dispersed PtO_x particles on the zeolite surface, as it was observed for Pd-modified zeolites prepared by LED [64]. The proportion of the metallic Pt⁰ state increases for monometallic samples with a higher Pt loading, which is typical for Pt and Pd catalysts formed by the LED method [62–65].

As previously noted, Co-modified zeolite Co/ZSM-5 may contain three types of Co species such as bare Co²⁺ cations, oxo-cations [Co_xO_y]ⁿ⁺ with n = 1, 2 in zeolite channels and cobalt oxides on the outer zeolite surface [17–19]. At the same time, cobalt (II) and (III) can be in both types of oxygen-containing particles ([Co_xO_y]ⁿ⁺ and oxides) [17]. The ratio of different metal form depends on the method of the Co introduction, metal loading, as well as on the number of ion-exchange positions in zeolite, i.e., on the Al content in zeolite framework. When the Co/Al ratio is less than 0.5, most of the cobalt is in the form of exchangeable Co²⁺ cations. In this case, the proportion of Co(II) is significant [18,19]. With an increase in the Co/Al ratio from 0.5 to 1, along with the former, oxo-cations containing Co(II) and Co(III) are formed inside the channels. With Co/Al > 1, the share of surface oxide particles is growing. As can be seen in Table 4, for zeolites Z-28 and Z-15, containing the same 4.5% of cobalt, the percentages of Co(III) and Co(II) turned out to be close, while the surface content of cobalt Co/(Si+Al) according to the XPS data is higher on the Z-28 zeolite, where a higher Co/Al = 1.4 ratio promotes the formation of surface oxides—mainly Co₃O₄, compared to the 4.5Co/Z-15, where this ratio is only 0.75 (Table 1). In accordance

with FTIR data (Figure 3) in the case of Z-15, a large proportion of the loaded cobalt is located in the zeolite channels, as was observed earlier for similar systems [17–19].

Differences in the Co distribution over the zeolite surface for different Si/Al are also confirmed by their textural characteristics (Table 2). With the introduction of 4.5% Co into zeolite Z-28, in contrast to Z-15, not only is there an observable decrease in the inner surface and pore size of the zeolite—which is associated with the penetration of cobalt into the channels—but there is also a slight increase in the outer surface due to the formation of oxide particles. In the 4.5Co/Z-28, a small band appears near 669 cm^{-1} due to stretching vibrations of the metal–oxygen bond in Co_3O_4 (Figure 3a). The outer surface of bimetallic Pt/Co/Z-28 zeolites grew even more noticeably.

For the samples with 0.01% Pt the fraction of metallic Pt^0 decreases, and the fraction of the less oxidized Co(II) state increases simultaneously as seen for 0.01Pt/4.5Co/Z-28. This is most likely due to the Pt–Co interaction during the synthesis. These changes are less noticeable for both 0.01Pt/4.5Co/Z-15 and 0.05Pt/2.5Co/Z-28, since in these cases most of the cobalt is inside the channels of the zeolite when Pt is mainly located on the outer zeolite surface. However, the fact that cobalt comes to the surface with the Pt introduction, and the Co/(Si+Al) ratio increases from 0.12 to 0.20 for 4.5Co/Z-15 and 0.01Pt/4.5Co/Z-15, respectively (Table 4), testifies in favor of the interaction of platinum and cobalt oxo-cations. The relative content of platinum on the surface of the bimetallic 0.01Pt/4.5Co/Z-15 sample is somewhat higher than in the monometallic Pt counterpart. This indicates that platinum mostly remains on the surface when the channels of the zeolite are largely occupied or blocked by cobalt species. The significant proportion of Pt^{II} with the maximum BE value present in the bimetallic samples (Table 4) can be associated not only with a strong metal–support interaction, but also with the formation of mixed oxo-complexes or oxides at the Pt–Co interfaces.

When cobalt was introduced after platinum deposition, the platinum content on the surface of 4.5Co/0.01 Pt/Z-28 turned out to be an order of magnitude lower than in samples with the reverse order of the introduction of components (Table 4). In this case, zeolite channels may be blocked by Pt nanoparticles deposited previously; Co mainly located on the outer zeolite as oxides; platinum was oxidized most strongly; and the ratio of Co(III) to Co(II) is close to that characteristic of supported $\text{Co}_3\text{O}_4/\text{SiO}_2$ [70].

The found differences in the structure of modified zeolites are reflected in their catalytic behavior. Even more significant changes in the electronic state of both metals occur under the influence of the PROX–CO reaction mixture, as will be shown below.

3.2. Catalytic Performance

3.2.1. Synergistic Effect of Pt and Co in CO-PROX

Temperature dependences of the CO to CO_2 conversion in a H_2 -rich mixture are shown in Figure 5, as an example of the 0.01Pt/4.5Co/Z-15 sample and its monometallic analogs. Temperature dependences of the CO conversion are extreme passing through a maximum when an undesirable reaction of the hydrogen oxidation starts, that reduces the selectivity of the process. The best catalytic behavior is determined by the highest degree of CO conversion at the lowest temperature. Another requirement for a good PROX catalyst is a wide temperature range (ΔT_{100}) of 100% CO conversion. It can be observed that the monometallic Pt-zeolite is the least active, which is not surprising due to such a low 0.01% Pt content. Only 78% CO conversion can be achieved at $210\text{ }^\circ\text{C}$. Cobalt-modified zeolite has slightly better properties, providing almost 100% conversion of CO at $190\text{ }^\circ\text{C}$, but with a further increase in temperature, the conversion drops sharply. This is associated not only with the side process of hydrogen oxidation, but also with a strong deactivation of cobalt-containing catalysts [19]. The best catalytic behavior is observed for a bimetallic 0.01Pt/4.5Co/Z-15, of which 100% conversion is already achieved at $110\text{ }^\circ\text{C}$ and decreases only to 97% as the temperature rises to $170\text{ }^\circ\text{C}$. Thus, a synergistic action of the two metals is observed, leading to a significant increase in the catalytic activity. The high activity of bimetallic Pt–Co catalysts of various structures has been repeatedly noted

in the literature [36–41]. However, such a strong improvement in catalytic properties of Co-modified zeolites with the introduction of such small (0.01%) Pt loading seems to be rather surprising.

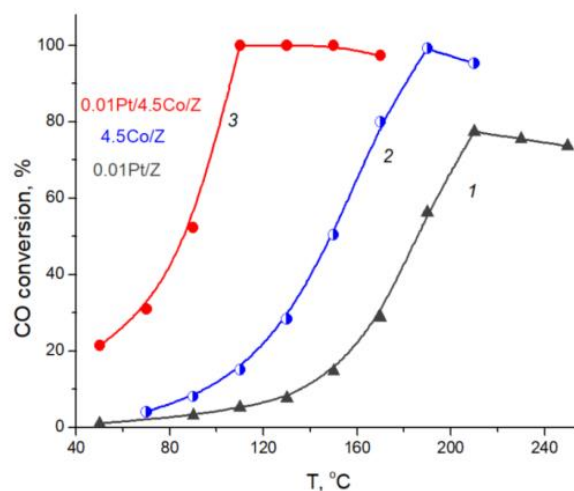


Figure 5. Temperature dependencies of the CO conversion for 0.01 Pt/Z-15 (1), 4.5Co/Z-15 (2) and 0.01Pt/4.5Co/Z-15 (3) samples.

3.2.2. Impact of Co/Al Ratio in 0.01Pt/Co/Z on Catalytic Performance

To design the most efficient catalysts with improved properties in CO-PROX, zeolites with different ratios of Si/Al (15, 28, and 40) were used, and the metal contents (0.01 and 0.05% Pt; 2.5 and 4.5% Co) were varied. The values of T_{50} of reaching the 50% CO conversion, the maximum achievable CO conversion, and temperature window ΔT_{100} to maintain 100% conversion (or the T_{max} temperature) for all tested bimetallic samples are collected in Table 5.

Table 5. The main catalytic characteristics of Pt/Co-modified zeolites: the temperatures corresponding to 50% and maximum conversion of CO (T_{50} and T_{max} , respectively) and temperature range to maintain 100% CO conversion (ΔT_{100}).

Catalyst	T_{50} , °C	CO_{max} , %	ΔT_{100} (T_{max}), °C
0.01Pt/2.5Co/Z-15	130	99	170
2.5Co/0.01Pt/Z-15	108	100	130–150
0.01Pt/4.5Co/Z-15	90	100	110–150
0.05Pt/4.5Co/Z-15	<50	100	50–150
0.01Pt/2.5Co/Z-28	97	100	130–170
0.01 Pt/4.5Co/Z-28	86	100	110–130
4.5Co/0.01Pt/Z-28	104	100	130
0.05Pt/2.5Co/Z-28	<50	100	60–150
0.01Pt/2.5Co/Z-40	100	100	130–150
0.01Pt/4.5Co/Z-40	95	100	130

To select the most suitable zeolite, the catalytic properties of the samples with the lowest loading of metals were compared. The difference in the catalytic behavior of 0.01Pt/2.5Co/Z on zeolites with a change in the Si/Al ratio is clearly visible from temperature dependences of the CO conversion presented in Figure 6. The catalyst 0.01Pt/2.5Co/Z-15 is the least active. Catalysts of the same composition on zeolites with higher Si/Al ratios (28 and 40) are similar in activity; however, the ΔT_{100} is wider for Z-28 (130–170 °C), while for Z-40 it is only 130–150 °C.

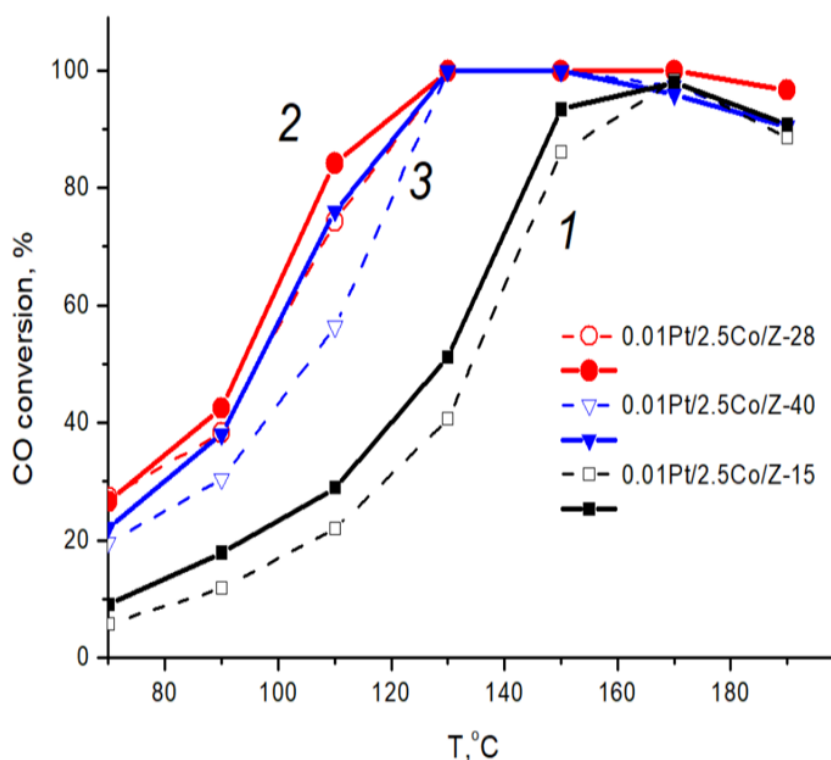


Figure 6. Temperature dependences of the CO conversion for the 0.01Pt/2.5Co/Z on zeolites with Si/Al: 15 (1), 28 (2), 40 (3). Shown are the data for heating–cooling cycles: dotted line and open symbols correspond to the heating cycle while solid line and solid symbols correspond to the cooling.

The difference in the catalytic behavior of the samples is most likely due to the different distribution of cobalt between the zeolite channels and outer surface determined by the ratios of Si/Al and Co/Al. The Co/Al ratio is less than 0.5 for the 0.01Pt/2.5Co/Z-15 catalyst (Table 1), and cobalt in this case is located in the zeolite channels mainly in the form of Co^{2+} cations and partially as oxo-cations $[\text{Co}_x\text{O}_y]^{n+}$, where $n = 1, 2$, containing both Co(II) and Co(III), as already discussed. In accordance with this data and previous studies [17–19], when the Co/Al ratio rises above 0.5, the fraction of bare Co^{2+} cations decreases, while the fractions of oxo-cations and surface cobalt oxide active in CO oxidation increases. Z-28 zeolite turns out to be the best in the series of 0.01Pt/2.5Co/Z catalysts because it provides the most favorable conditions for the interaction of Pt nanoparticles deposited by the LED with both types of oxidized Co species. Co^{2+} cations located predominantly inside zeolite channels in 0.01Pt/2.5Co/Z-15 are less involved in interactions with platinum nanoparticles on the zeolite surface; therefore, such samples are less active in CO oxidation. This assumption can be confirmed by the fact that the activity of 2.5Co/0.01Pt/Z-15 catalyst obtained by the reverse order of the component introduction improved. Indeed, where Pt nanoparticles were first deposited on the surface by LED, and then cobalt was introduced via impregnation of Pt/Z-15, the value of T_{50} reduced by 20 °C and ΔT_{100} widened to 130–150 °C. This operating window became closer to that of the more active catalysts on Z-28 and Z-40. However, in contrast to the best 0.01Pt/2.5Co/Z-28 stable in temperature window between 130–170 °C, the conversion on Z-40 begins to noticeably decrease after 150 °C. In this case, Co/Al is above 1 even at 2.5% Co, and a significant amount of Co_3O_4 oxide nanoparticles are formed on the zeolite surface. They are known [19,70,74] to be active in the oxidation of hydrogen and are rapidly deactivated by the resulting water. The effect of the presence of a significant amount of oxide particles on the support surface is even more pronounced when the cobalt content is increased to 4.5%. As can be seen in Table 5, the 100% CO conversion on 0.01Pt/4.5Co/Z-40 starts to already decrease after 130 °C.

Zeolites with an increased cobalt content are more active: T_{50} is reduced for 0.01Pt/4.5Co/Z in comparison with 2.5Co analogs. However, in this series, the order of catalytic activity of the samples with different Si/Al ratio has changed. The catalyst prepared on zeolite Z-15 now has the highest activity and stability. As can be seen in Table 5, the temperature window ΔT_{100} in this case expands to 110–170 °C in the region both of low and high temperatures. At the same time, for 0.1Pt/4.5Co/Z-28 the region of ΔT_{100} is narrower and is only 110–130 °C. Upon further increase in Si/Al to 40, the 100% CO conversion was only achieved at 130 °C.

Thus, it can be concluded once again that the initial Co state and its distribution over the zeolite surface plays an important role in the catalytic performance. For two different samples of 0.01Pt/4.5Co/Z-15 and 0.01Pt/2.5Co/Z-28, the ratio of Co/Al are close to 0.75 and the main part of cobalt is located here in the form of oxo-cations [17–19]. However, on the first of them, containing 4.5% Co on Z-15, the total amount of Co oxo-cations is higher than on the second, containing only 2.5% Co. With an increase in Co/Al, the proportion of Co oxide particles on the zeolite surface increases, and accordingly, the contribution of the side reaction of hydrogen oxidation increases. This reduces the operating window ΔT_{100} for the 0.01Pt/4.5Co/Z systems under consideration for Z-28 and Z-40 zeolites in comparison with Z-15. Apparently, with such a catalyst composition of 0.01Pt/4.5Co/Z, it is the Z-15 zeolite that provides the optimal distribution of Co between oxo-cations inside the zeolite channels and oxides, which leads to better Pt-Co interaction.

The importance of involving both oxygen-containing forms of Co in the interaction with Pt has been proved by the results of comparing the properties of catalysts 0.01Pt/4.5Co/Z-28 and 4.5Co/0.01Pt/Z-28 with different order of the introduction of components. When cobalt was introduced over pre-deposited platinum, changes in the electronic state of Pt and Co are even more significant (Table 4). The Pt^0 fraction stronger decreased to 8%, and the ratio of Co(III) and Co(II) states became close to this for Co_3O_4 [70]. In this case, cobalt is located predominantly in the form of a surface Co_3O_4 oxide; the activity of such a sample turned out to be lower compared to 0.01Pt/4.5Co/Z-28 (Table 5).

Thus, between samples with the 0.01% Pt content, two 0.01Pt/4.5Co/Z-15 and 0.01Pt/2.5Co/Z-28 catalysts are the best in terms of their activity and the ΔT_{100} operating window. In order to improve the catalytic behavior and to lower the temperature of CO-PROX, the platinum content in the two most promising composites was increased to 0.05 wt.%.

3.2.3. Pt content Influence on Catalytic Properties

As can be seen in Table 5, both catalysts 0.05Pt/4.5Co/Z-15 and 0.05Pt/2.5Co/Z-28 are highly active and stable. As seen in Figure 7, after heating even to low temperatures (50–70 °C) in the reaction medium, the 0.05Pt/4.5Co/Z-15 activity increases to 100% at 50–150 °C, and only slightly reduces to 97 % at 170 °C. Similar behavior was also observed for 0.05Pt/2.5Co/Z-28, where the operating temperature range (ΔT_{100}) is significantly extended for both catalysts. As seen in Figure 8, these catalysts with the optimal composition provide the 100% CO conversion within at least 8 h.

The increase of catalytic activity during the first heating (Figures 6 and 7) may be associated with a catalyst evolution under the action of reaction mixture. In accordance with XPS data (Table 4), the electronic states of both metals noticeably change during the catalytic process and the fraction of oxidized platinum reduces noticeably. Interestingly, at the same time the share of the more oxidized Co(III) state increases. The same changes are also observed in spent 0.01Pt/4.5Co/Z-15 samples with the lower Pt loading. The reduction of platinum under the action of a reducing reaction mixture, including CO and H_2 , seems to be expected. It is important here that after heating in such a mixture, a significant proportion of oxidized platinum is retained. It is the simultaneous presence of the metallic Pt^0 and partially oxidized $Pt^{\delta+}$ phases that is responsible for the high activity of platinum catalysts in the CO oxidation [23,24,44,65,75]. The growth of the Co (III) fraction under the PROX conditions seems quite surprising. Most likely, under the action of the reaction mixture, the reconstruction and redistribution of cobalt species in the zeolite structure can occur.

As can be seen in Table 4, the cobalt content on the surface in the spent catalysts increases significantly, which is especially noticeable for a sample with a large 0.05% Pt content.

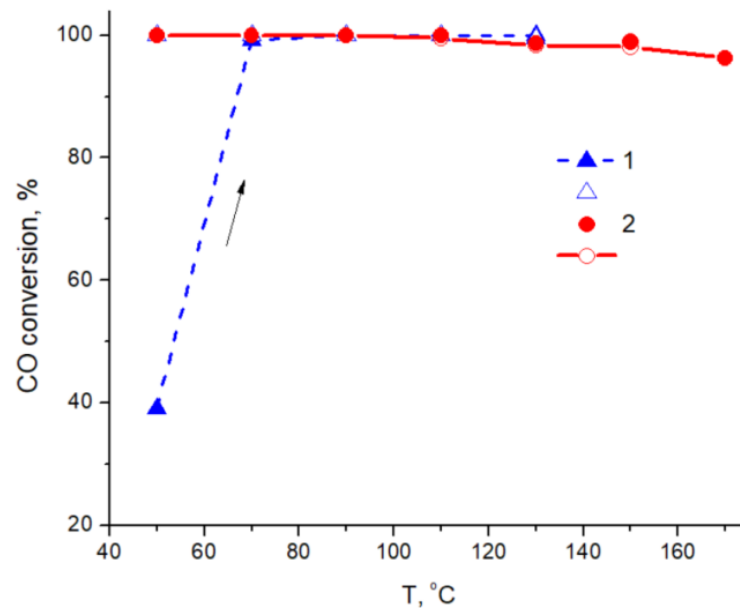


Figure 7. Temperature dependences of CO conversion on 0.05Pt/4.5Co/Z-15 in successive heating-cooling cycles (1 and 2). Shown are the data for two heating-cooling cycles: dotted line and solid symbols correspond to the heating cycle, while solid line and open symbols correspond to the cooling. The up arrow denotes heating.

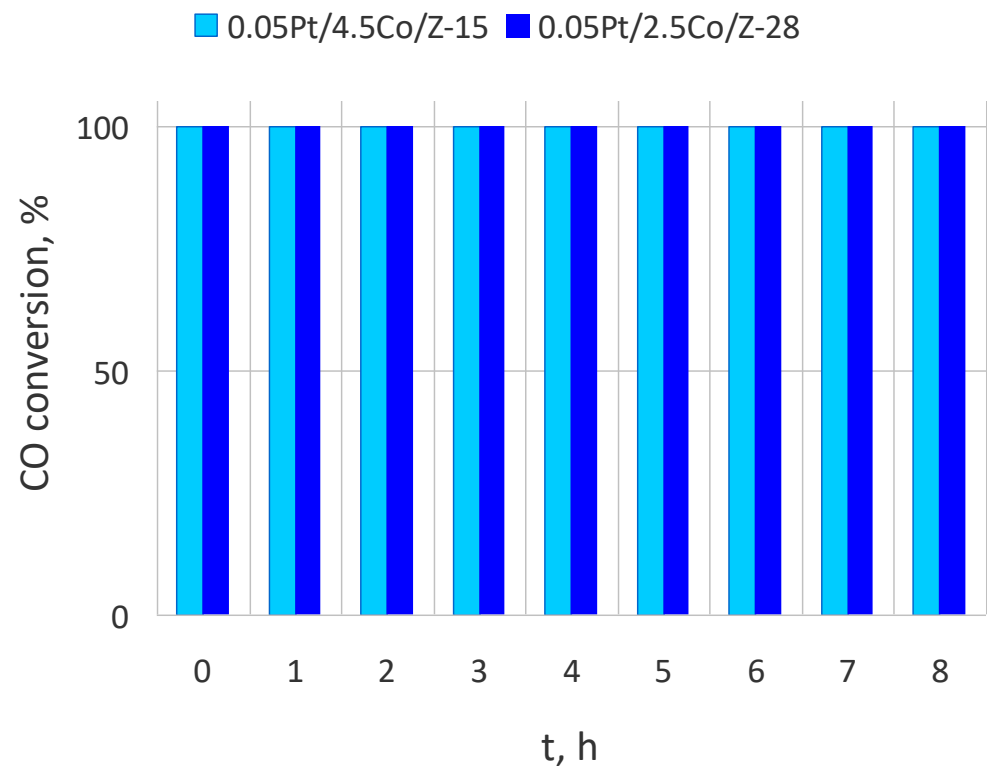


Figure 8. CO conversion over two Pt/Co/Z catalysts at 70 °C as a function of time.

Close Pt contact with Co oxo-cations containing Co (II) and Co (III) changes the electronic state of both metals. As recently found, the strong interaction between Pt and Co_3O_4 resulted in an increase of the Pt^0 fraction in Pt-Co catalysts [76]. Similar results were

obtained for CoO_x decorated with platinum on alumina [41] and carbon supports [77]. Another reason for the growth of a more oxidized Co(III) state may be a reconstruction of Co oxidized species, as it was observed during redox treatments of Co_3O_4 [13]. An easy reducibility and low-temperature re-oxidation of bimetallic Pt-containing catalysts correlates with their higher activity in comparison with monometallic ones [35]. Furthermore, the new electronic states of both metals with a predominance of partially reduced platinum and the most oxidized state of cobalt favorable for the catalytic CO oxidation are formed under the action of the reaction medium. The close interaction of Pt and Co species in different oxidation states provides the organization of new active centers at the Pt-Co interface. It is known that the CO adsorption is weakened and O_2 is activated on such sites, and thus, this is the reason for the synergistic effect often observed in Pt-Co systems [36–41,75–77]. However, two important features are discovered in this work. First, we discover the effect of small additions of highly dispersed Pt particles on the structure and catalytic properties of Co-modified zeolites. In this instance, the LED method for size selective deposition of platinum particles with optimal catalysis size of about 2 nm turned out to be very useful. Second, we discover that it is not only cobalt oxides on the zeolite surface that are involved in interactions with platinum, but also oxo-cationic Co complexes stabilized in the channels. Their interaction with finely dispersed PtOx particles provides the unusually high activity and stability of the designed Pt low loaded catalysts at moderate temperatures. The high Pt dispersion in catalyst prepared by LED may be responsible for the high CO selectivity, as was observed for low loaded 0.3% Pt catalysts promoted with 12%Ce on alumina [43]. In addition, the preservation of oxidized platinum under the process conditions and a decrease in the proportion of Co(II) reduces the dissociative adsorption of hydrogen and increases the selectivity of CO oxidation.

In this study, an improvement in activity and selectivity for Pt-Co supported catalysts with ultralow 0.01–0.05 wt% Pt content was discovered for the first time. Operating temperature ranges between 65 and 130 °C were previously found only for samples with a platinum content of 1% or more [36,37,39–41]. A further temperature increase generates a decrease in the CO conversion. Only a few successful attempts to reduce platinum content are known—for example, highly active catalysts with ~0.8% Pt have been synthesized via a selective atomic layer platinum deposition on supported CoO_x nanoclusters [38]. A recently published work [77] reports that full CO conversion for the Pt-Fe-NaY catalyst was observed at 75 °C, but only at a metal loading of 0.75 wt.% and above; attempts to reduce the content of platinum led to a loss of activity. In accordance with published data and our results, it can be concluded that the design of high-performance PROX catalysts should be based on the study of the relationship between their structure and properties, a rational choice of the most appropriate synthesis method, and the type of zeolite and promoting metal, should be conducted.

4. Conclusions

Original method of laser electrodispersion (LED) was applied for the selective deposition of highly dispersed Pt particles of 1.7 nm on the surface of Co-zeolite pre-modified by impregnation with 2.5 or 4.5 wt.% Co. The use of HZSM-5 zeolite with different ratio Si/Al makes it possible to stabilize Co in the form of oxo-cations in zeolite channels that are more active in the CO oxidation compared with surface Co_3O_4 and CoO oxides and to achieve the best Pt-Co contacts. The fractions of different forms of oxidized Co species and the electronic state of both metals depend on the Co/Al ratio. Prepared by this means, Pt-Co/zeolites with low Pt loading (0.01–0.05 wt.%) are unusually active and stable under the CO-PROX conditions. For two 0.05Pt/4.5Co/Z-15 and 0.05Pt/2.5Co/Z-28 catalysts with the best properties, the 100% CO conversion achieves and maintains for a long time in the temperature range of 50–150 °C. This provides the necessary purification of hydrogen from CO and even overlaps the operating window of 60–80 °C of proton exchange membrane fuel cells (PEMFC). In accordance with XPS studies, new active sites are formed at the Pt-Co interfaces under the action of reaction mixture. It is the use of zeolite that promotes

the formation and stabilization of partially oxidized platinum and the most oxidized Co(III) in the close contact on the surface. The weak CO adsorption at the metal-oxide interface leaving sites for the O₂ activation and an additional source of oxygen from neighboring Co oxides or oxo-cations provides the improved catalytic behavior of produced catalysts. As far as we know, these are the best results for catalysts with such a low Pt loading. This approach may be applied to design highly active catalysts for the oxidation of CO and other hazardous air pollutants.

Supplementary Materials: The following supporting information can be downloaded at: <https://www.mdpi.com/article/10.3390/hydrogen4010011/s1>, Figure S1: XRD patterns of the parent HZSM-5 and 0.05Pt/2.5Co/Z-28 and 4.5Co/Z-28 catalysts; Figure S2: (a,b) TEM images of 0.01Pt/Z-15; Figure S3: TEM images (a, b) of 0.05Pt/Z-28 and (c, d) of 4.5Co/Z-28; Figure S4: (a) TEM image and EDX element distribution maps of (b) Si, (c) Co and (d) Pt of 0.01Pt/4.5Co/Z-15; Figure S5: (a) TEM image and (b) particle size distribution of 0.01Pt/4.5Co/Z-15; Figure S6: (a) TEM image and EDX element distribution maps of (b) Al, (c) Si, (d) O, (e) Co and (f) Pt of 4.5Co/0.01Pt/Z-28; Figure S7: (a) TEM image, (b) EDX spectrum, and (c) particle size distribution of 4.5Co/0.01Pt/Z-28; Figure S8: SEM image (a) and EDX element distribution maps of (b) Co and (c) Pt of 0.05Pt/2.5Co/Z-28.

Author Contributions: Conceptualization, M.S. and T.R.; methodology and validation, S.G.; formal analysis, S.N.; investigation, O.U., I.K., D.Y.; writing—original draft preparation, T.R.; writing—review and editing, M.S. All authors have read and agreed to the published version of the manuscript.

Funding: This research received no external funding.

Institutional Review Board Statement: Not applicable.

Informed Consent Statement: Not applicable.

Data Availability Statement: Data is contained within the article.

Acknowledgments: The catalysts were synthesized by LED within the framework of the State Assignment to the Ioffe Physico-Technical Institute, Russian Academy of Sciences (Project No. 0040-2019-0010). The chemical synthesis and structural studies were performed within the framework of the State Assignment to the Lomonosov Moscow State University (Project No. AAAA-A21-121011590090-7). Catalysts were tested within the framework of the State Assignment to the Semenov Federal Research Center for Chemical Physics, Russian Academy of Sciences (Project No. 122040500058-1 “Physics and chemistry of new nanostructured systems and composite materials with desired properties”). Structural studies were carried out using the equipment purchased within the framework of the Lomonosov Moscow State University Development Program. The authors are grateful to K. Maslakov for help in carrying out these studies.

Conflicts of Interest: The authors declare no conflict of interest.

References

1. Pourrahmani, H.; Yavarinasab, A.; Siavashi, M.; Matian, M.; Vanherle, J. Progress in the proton exchange membrane fuel cells (PEMFCs) water/thermal management: From theory to the current challenges and real-time fault diagnosis methods. *Energy Rev.* **2022**, *1*, 100002. [[CrossRef](#)]
2. Jing, P.; Gong, X.; Liu, B.; Zhang, J. Recent advances in synergistic effect promoted catalysts for preferential oxidation of carbon monoxide. *Catal. Sci. Technol.* **2020**, *10*, 919–934. [[CrossRef](#)]
3. Park, E.D.; Lee, D.; Lee, H.C. Recent progress in selective CO removal in a H₂-rich stream. *Catal. Tod.* **2009**, *139*, 280–290. [[CrossRef](#)]
4. Liu, J.; Hensley, A.J.R.; Giannakakis, G.; Therrien, A.J.; Sukkar, A.; Schilling, A.C.; Groden, K.; Ulumuddin, N.; Hannagan, R.T.; Ouyang, M.; et al. Developing single-site Pt catalysts for the preferential oxidation of CO: A surface science and first principles-guided approach. *Appl. Catal. B* **2021**, *284*, 119716. [[CrossRef](#)]
5. Du, X.; Lang, Y.; Cao, K.; Yang, J.; Cai, Y.; Shan, B.; Chen, R. Bifunctionally faceted Pt/Ru nanoparticles for preferential oxidation of CO in H₂. *J. Catal.* **2021**, *396*, 148–156. [[CrossRef](#)]
6. Nguen, T.-S.; Morfin, F.; Aouine, M.; Bosselet, F.; Roussert, J.-L.; Laurent, P. Trends in the CO oxidation and PROX performances of the platinum-group metals supported on ceria. *Catal. Tod.* **2015**, *253*, 106–114. [[CrossRef](#)]
7. Watanabe, M.; Uchida, H.; Ohkubo, K.; Igarashi, H. Hydrogen purification for fuel cells: Selective oxidation of carbon monoxide on Pt-Fe/zeolite catalysts. *Appl. Catal. B* **2003**, *46*, 595–600. [[CrossRef](#)]

8. Marino, F.; Descorme, C.; Duprez, D. Noble metal catalysts for the preferential oxidation of carbon monoxide in the presence of hydrogen (PROX). *Appl. Catal. B* **2004**, *54*, 59–66. [[CrossRef](#)]
9. Rosso, I.; Galletti, C.; Saracco, G.; Garrone, E.; Specchia, V. Development of A zeolites-supported noble-metal catalysts for CO preferential oxidation: H₂ gas purification for fuel cell. *Appl. Catal. B* **2004**, *48*, 195–203. [[CrossRef](#)]
10. Zlotea, C.; Oumella, Y.; Provosk, K.; Morfin, F.; Piccolo, L. Role of hydrogen absorption in supported Pd nanocatalysts during CO-PROX: Insights from operando X-ray absorption spectroscopy. *Appl. Catal. B* **2018**, *237*, 1059–1065. [[CrossRef](#)]
11. Marino, F.; Descorme, C.; Duprez, D. Supported base metal catalysts for the preferential oxidation of carbon monoxide in the presence of excess hydrogen (PROX). *Appl. Catal. B* **2005**, *58*, 175–183. [[CrossRef](#)]
12. Li, J.; Lei, Y.; Guo, Z.; Li, G.; Chen, X.; Zhou, F. Temperature-dependent reaction pathways of CO oxidation and the application as monolithic catalysts for Co₃O₄ nanorods. *Appl. Catal. A* **2019**, *587*, 117191. [[CrossRef](#)]
13. Yang, J.; Guo, J.; Wang, Y.; Wang, T.; Gu, J.; Peng, L.; Xue, N.; Zhu, Y.; Guo, X.; Ding, W. Reduction-oxidation pretreatment enhanced catalytic performance of Co₃O₄/Al₂O₃ over CO oxidation. *Appl. Surf. Sci.* **2018**, *453*, 330–335. [[CrossRef](#)]
14. Royer, S.; Duprez, D. Catalytic oxidation of carbon monoxide over transition metal oxides. *ChemCatChem* **2011**, *3*, 24–65. [[CrossRef](#)]
15. Arango-Diaz, A.; Cecilia, J.A.; Marrero-Jerez, J.; Nuñez, P.; Jiménez-Jiménez, J.; Rodríguez-Castellón, E. Freeze-dried Co₃O₄-CeO₂ catalysts for the preferential oxidation of CO with the presence of CO₂ and H₂O in the feed. *Ceram. Int.* **2016**, *46*, 7462–7474. [[CrossRef](#)]
16. Gawade, P.; Bayram, B.; Alexander, A.-M.C.; Ozkan, U.S. Preferential oxidation of CO (PROX) over CoO_x/CeO₂ in hydrogen-rich streams: Effect of cobalt loading. *Appl. Catal. B* **2012**, *128*, 21–32. [[CrossRef](#)]
17. Shilina, M.I.; Rostovshchikova, T.N.; Nikolaev, S.A.; Udalova, O.V. Polynuclear Co-oxo cations in the catalytic oxidation of CO on Co-modified ZSM-5 zeolites. *Mater. Chem. Phys.* **2019**, *223*, 287–298. [[CrossRef](#)]
18. Shilina, M.; Udalova, O.; Krotova, I.; Ivanin, I.; Boichenko, A. Oxidation of carbon monoxide on Co/Ce-modified ZSM-5 zeolites: Impact of mixed Oxo-Species. *ChemCatChem* **2020**, *12*, 2556–2568. [[CrossRef](#)]
19. Ivanin, I.A.; Krotova, I.N.; Udalova, O.V.; Zanaevskina, K.L.; Shilina, M.I. Synergistic catalytic effect of cobalt and cerium in the preferential oxidation of carbon monoxide on modified Co/Ce/ZSM-5 Zeolites. *Kin. Cat.* **2021**, *62*, 798–811. [[CrossRef](#)]
20. McClure, S.M.; Goodman, D.W. New insights into catalytic CO oxidation on Pt-group metals at elevated pressures. *Chem. Phys. Lett.* **2009**, *469*, 1–13. [[CrossRef](#)]
21. Lin, J.; Wang, X.; Zhang, T. Recent progress in CO oxidation over Pt-group-metal catalysts at low temperatures. *Chin. J. Catal.* **2016**, *37*, 1805–1813. [[CrossRef](#)]
22. Neumann, S.; Gutmann, T.; Buntkowsky, G.; Paul, S.; Thiele, G.; Sievers, H.; Blaumer, M.; Kurz, S. Insights into the reaction mechanism and particle size effects of CO oxidation over supported Pt nanoparticle catalysts. *J. Catal.* **2019**, *377*, 662–672. [[CrossRef](#)]
23. Chen, X.; Chen, J.; Zhao, Y.; Chen, M.; Wan, H. Effect of dispersion on catalytic performance of supported Pt catalysts for CO oxidation. *Chin. J. Catal.* **2012**, *33*, 1901–1905. [[CrossRef](#)]
24. Chen, Y.; Lin, J.; Li, L.; Pan, X.; Wang, X.; Zhang, T. Local structure of Pt species dictates remarkable performance on Pt/Al₂O₃ for preferential oxidation of CO in H₂. *Appl. Catal. B* **2021**, *282*, 119588. [[CrossRef](#)]
25. Pakharukova, V.P.; Pakharukov, I.Y.; Bukhtiyarov, V.I.; Parmon, V.N. Alumina-supported platinum catalysts: Local atomic structure and catalytic activity for complete methane oxidation. *Appl. Catal. A* **2014**, *486*, 12–18. [[CrossRef](#)]
26. Feng, C.; Liu, X.; Zhu, T.; Hu, Y.; Tian, M. Catalytic oxidation of CO over Pt/TiO₂ with low Pt loading: The effect of H₂O and SO₂. *Appl. Catal. A* **2021**, *622*, 118218. [[CrossRef](#)]
27. Qiao, B.; Wang, A.; Li, L.; Lin, Q.; Wei, H.; Liu, J.; Zhang, T. Ferric oxide-supported Pt subnano clusters for preferential oxidation of CO in H₂-rich gas at room temperature. *ACS Catal.* **2014**, *4*, 2113–2117. [[CrossRef](#)]
28. Lang, R.; Du, X.; Huang, Y.; Jiang, X.; Zhang, Q.; Guo, Y.; Liu, K.; Qiao, B.; Wang, A.; Zhang, T. Single-atom catalysts based on the metal–oxide interaction. *Chem. Rev.* **2020**, *120*, 11986–12043. [[CrossRef](#)]
29. Cao, S.; Zhao, Y.; Lee, S.; Yang, S.; Liu, J.; Giannakakis, G.; Li, M.; Ouyang, M.; Wang, D.; Sykes, E.C.H.; et al. High-loading single Pt atom sites [Pt-O (OH)_x] catalyze the CO PROX reaction with high activity and selectivity at mild conditions. *Sci. Adv.* **2020**, *6*, eaba3809. [[CrossRef](#)]
30. Niu, T.; Zhao, W.W.; Liu, G.L.; Cao, A.; Zhang, L.H.; Liu, Y. The graphene-meso-macro-porous SiO₂ supported Pt-Ni alloy nanocatalyst for preferential oxidation of CO in H₂-rich gases. *Int. J. Hydrog. Energy* **2014**, *39*, 18929–18939. [[CrossRef](#)]
31. Teschner, D.; Wootscha, A.; Paál, Z. Preferential CO oxidation in hydrogen (PROX) on unsupported PtSn catalyst. *Appl. Catal. A* **2012**, *411–412*, 31–34. [[CrossRef](#)]
32. Tripathi, A.; Hareesh, C.; Sinthika, S.; Andersson, G.; Thapa, R. CO oxidation on Pt based binary and ternary alloy nanocatalysts: Reaction pathways and electronic descriptor. *Appl. Surf. Sci.* **2020**, *528*, 146964. [[CrossRef](#)]
33. Zhang, H.; Liu, X.; Zhang, N.; Zheng, J.; Zheng, Y.; Li, Y.; Zhong, C.-J.; Chen, B.H. Construction of ultrafine and stable PtFe nano-alloy with ultra-low Pt loading for complete removal of CO in PROX at room temperature. *Appl. Catal. B* **2016**, *180*, 237–245. [[CrossRef](#)]
34. Potemkin, D.I.; Filatov, E.Y.; Zadesenets, A.V.; Gorlova, A.M.; Nikitina, N.A.; Pichugina, D.A. A comparative study of CO preferential oxidation over Pt and Pt_{0.5}Co_{0.5} nanoparticles: Kinetic study and quantum-chemical calculations. *Mater. Lett.* **2020**, *260*, 126915. [[CrossRef](#)]

35. Mohamed, Z.; Dasireddy, V.D.B.C.; Singh, S.; Fiedrich, H.B. The preferential oxidation of CO in hydrogen rich streams over platinum doped nickel oxide catalysts. *Appl. Catal. B* **2016**, *180*, 687–697. [[CrossRef](#)]
36. Wang, C.X.; Zhang, L.; Liu, Y. Aluminumphosphate molecular sieves supported Pt–Co catalysts for the preferential oxidation of CO in H₂-rich gases. *Appl. Catal. B* **2013**, *136–137*, 48–55. [[CrossRef](#)]
37. Li, H.; Yu, X.; Tu, S.-T.; Yan, J.; Wang, Z. Catalytic performance and characterization of Al₂O₃-supported Pt–Co catalyst coatings for preferential CO oxidation in a micro-reactor. *Appl. Catal. A* **2010**, *387*, 215–223. [[CrossRef](#)]
38. Cai, J.; Liu, Z.; Cao, K.; Lang, Y.; Chu, S.; Shan, B.; Chen, R. Highly dispersed Pt studded on CoO_x nanoclusters for CO preferential oxidation in H₂. *J. Mater. Chem. A* **2020**, *8*, 10180–10187. [[CrossRef](#)]
39. Potemkin, D.I.; Filatov, E.Y.; Zadesenets, A.V.; Snytnikov, P.V.; Shubin, Y.V.; Sobyenin, V.A. Preferential CO oxidation over bimetallic Pt–Co catalysts prepared via double complex salt decomposition. *Chem. Eng. J.* **2012**, *207–208*, 683–689. [[CrossRef](#)]
40. Wang, C.; Li, B.; Lin, H.; Yuan, Y. Carbon nanotube-supported Pt–Co bimetallic catalysts for preferential oxidation of CO in a H₂-rich stream with CO₂ and H₂O vapor. *J. Power Sources* **2012**, *202*, 200–208. [[CrossRef](#)]
41. Nunez, N.E.; Bideberripe, H.P.; Mizrahi, M.; Ramallo-López, J.M.; Casella, M.L.; Siri, G.J. CO selective oxidation using Co-promoted Pt/γ-Al₂O₃ catalysts. *Int. J. Hydrog. Energy* **2016**, *41*, 19005–19013. [[CrossRef](#)]
42. Freund, H.-J.; Meijer, G.; Scheffler, M.; Schlögl, R.; Wolf, M. CO Oxidation as a Prototypical Reaction for Heterogeneous Processes. *Angew. Chem. Int. Ed.* **2011**, *50*, 10064. [[CrossRef](#)] [[PubMed](#)]
43. Paz, D.S.; Damyanov, S.; Borges, L.R.; Santos, J.B.O.; Bueno, J.M.C. Identifying the adsorbed active intermediates on Pt surface and promotion of activity through the redox CeO₂ in preferential oxidation of CO in H₂. *Appl. Catal. A* **2017**, *548*, 164–178. [[CrossRef](#)]
44. Teschner, D.; Wootsch, A.; Pozdnyakova-Tellinger, O.; Kröhnert, J.; Vass, E.M.; Hävecker, M.; Zafeiratos, S.; Schnörch, P.; Jentoft, P.C.; Knop-Gericke, A.; et al. Partial pressure dependent in situ spectroscopic study on the preferential CO oxidation in hydrogen (PROX) over Pt/ceria catalysts. *J. Catal.* **2007**, *249*, 318–327. [[CrossRef](#)]
45. Komatsu, T.; Tamura, A. Pt₃Co and PtCu intermetallic compounds: Promising catalysts for preferential oxidation of CO in excess hydrogen. *J. Catal.* **2008**, *258*, 306–314. [[CrossRef](#)]
46. Lopez, A.; Navascues, N.; Mallada, R.; Irusta, S. Pt–CoO_x nanoparticles supported on ETS-10 for preferential oxidation of CO reaction. *Appl. Catal. A* **2016**, *528*, 86–92. [[CrossRef](#)]
47. Cuenya, B.R. Synthesis and catalytic properties of metal nanoparticles: Size, shape, support, composition, and oxidation state effects. *Thin Solid Films* **2010**, *518*, 3127–3150. [[CrossRef](#)]
48. Uzio, D.; Berhault, G. Factors governing the catalytic reactivity of metallic nanoparticles. *Catal. Rev.* **2010**, *52*, 106–131. [[CrossRef](#)]
49. Lokteva, E.S.; Golubina, E.V. Metal-support interactions in the design of heterogeneous catalysts for redox processes. *Pure Appl. Chem.* **2019**, *91*, 609. [[CrossRef](#)]
50. Xu, J.; Xu, X.-C.; Ouyang, L.; Yang, X.-J.; Mao, W.; Su, J.; Han, Y.-F. Mechanistic study of preferential CO oxidation on a Pt/NaY zeolite catalyst. *J. Catal.* **2012**, *287*, 114–123. [[CrossRef](#)]
51. Sebastian, V.; Irusta, S.; Mallada, R.; Santamaría, J. Microreactors with Pt/zeolite catalytic films for the selective oxidation of CO in simulated reformer streams. *Catal. Tod.* **2009**, *147S*, S10–S16. [[CrossRef](#)]
52. Sebastian, V.; Irusta, S.; Mallada, R.; Santamaría, J. Selective oxidation of CO in the presence of H₂, CO₂ and H₂O on different zeolite-supported Pt catalysts. *Appl. Catal. A* **2009**, *366*, 242–251. [[CrossRef](#)]
53. Tian, J.; Wang, C.; Wu, J.; Sun, D.; Li, Q. Enhancing water resistance of Pt nanoparticles by tailoring microenvironment of hollow ZSM-5 for efficient benzene oxidation. *Chem. Eng. J.* **2023**, *451*, 138351. [[CrossRef](#)]
54. Guo, J.; Ding, C.; Ma, Z.; Ma, L.; Wang, J.; Shangguan, J.; Yuan, Q.; Zhao, M.; Li, Y.; Wang, M.; et al. Highly dispersed and stable Pt clusters encapsulated within ZSM-5 with aid of sodium ion for partial oxidation of methane. *Fuel* **2021**, *289*, 119839. [[CrossRef](#)]
55. Kong, F.; Li, G.; Wang, J.; Shi, Y.; Zhou, R. Promoting effect of acid sites in hierarchical porous Pt/ZSM-5 catalysts for low-temperature removal of VOCs. *Appl. Surf. Sci.* **2022**, *606*, 154888. [[CrossRef](#)]
56. Jiang, Z.; Chen, D.; Deng, W.; Guo, L. Different morphological ZSM-5 zeolites supported Pt catalysts for toluene catalytic combustion. *Chem. Phys. Impact.* **2022**, *5*, 100134. [[CrossRef](#)]
57. El-Bahy, Z.M.; Alotaibi, M.T.; El-Bahy, S.M. CO oxidation and 4-nitrophenol reduction over ceria-promoted platinum nanoparticles impregnated with ZSM-5 zeolite. *J. Rare Earths* **2022**, *40*, 1247–1254. [[CrossRef](#)]
58. Wang, J.; Guo, X.; Shi, Y.; Zhou, R. Synergistic effect of Pt nanoparticles and micro-mesoporous ZSM-5 in VOCs low-temperature removal. *J. Environ. Sci.* **2021**, *107*, 87–97. [[CrossRef](#)]
59. Babucci, M.; Guntida, A.; Gates, B.C. Atomically dispersed metals on well-defined supports including zeolites and metal–organic frameworks: Structure, bonding, reactivity, and catalysis. *Chem. Rev.* **2020**, *120*, 11956–11985. [[CrossRef](#)]
60. Michalak, W.D.; Krier, J.M.; Alayoglu, S.; Shin, J.-Y.; An, K.; Komvopoulos, K.; Liu, Z.; Somorjai, G.A. CO oxidation on PtSn nanoparticle catalysts occurs at the interface of Pt and Sn oxide domains formed under reaction conditions. *J. Catal.* **2014**, *312*, 17–25. [[CrossRef](#)]
61. Forsythe, R.C.; Cox, C.P.; Wilsey, M.K.; Müller, A.M. Pulsed Laser in Liquids Made Nanomaterials for Catalysis. *Chem. Rev.* **2021**, *121*, 7568–7637. [[CrossRef](#)]
62. Rostovshchikova, T.N.; Lokteva, E.S.; Shilina, M.I.; Golubina, E.V.; Maslakov, K.I.; Krotova, I.N.; Bryzhin, A.A.; Tarkhanova, I.G.; Udalova, O.V.; Kozhevnikov, V.M.; et al. Laser electrodispersion of metals for the synthesis of nanostructured catalysts: Achievements and prospects. *Russ. J. Phys. Chem. A* **2021**, *95*, 451–474. [[CrossRef](#)]

63. Bryzhin, A.A.; Golubina, E.V.; Maslakov, K.I.; Lokteva, E.S.; Tarkhanova, I.G.; Gurevich, S.A.; Yavsin, D.A.; Rostovshchikova, T.N. Bimetallic nanostructured catalysts prepared by laser electrodispersion: Structure and activity in redox reactions. *ChemCatChem* **2020**, *12*, 4396–4405. [[CrossRef](#)]
64. Rostovshchikova, T.N.; Nikolaev, S.A.; Krotova, I.N.; Maslakov, K.I.; Udalova, O.V.; Gurevich, S.A.; Yavsin, D.A.; Shilina, M.I. ZSM-5 and BEA zeolites modified with Pd nanoparticles by laser electrodispersion. The structure and catalytic activity in CO and CH₄ oxidation. *Russ. Chem. Bull.* **2022**, *71*, 1179–1193. [[CrossRef](#)]
65. Golubina, E.V.; Rostovshchikova, T.N.; Lokteva, E.S.; Maslakov, K.I.; Nikolaev, S.A.; Shilina, M.I.; Gurevich, S.A.; Kozhevnikov, V.M.; Yavsin, D.A.; Slavinskaya, E.M. Role of surface coverage of alumina with Pt nanoparticles deposited by laser electrodispersion in catalytic CO oxidation. *Appl. Surf. Sci.* **2021**, *536*, 147656. [[CrossRef](#)]
66. Rostovshchikova, T.N.; Shilina, M.I.; Gurevich, S.A.; Yavsin, D.A.; Veselov, G.B.; Vedyagin, A.A. New approaches to the synthesis of ultralow-palladium automotive emission control catalysts. *Dokl. Phys. Chem.* **2022**, *506*, 123–130. [[CrossRef](#)]
67. Chupin, C.; van Veen, A.C.; Konduru, M.; Deprés, J.; Mirodatos, C. Identity and location of active species for NO reduction by CH₄ over Co-ZSM-5. *J. Catal.* **2006**, *241*, 103–114. [[CrossRef](#)]
68. Coudurier, G.; Naccache, C.; Viedrine, J.C. Uses of I.R. spectroscopy in identifying ZSM zeolite structure. *J. Chem. Soc. Chem. Commun.* **1982**, *24*, 1413–1415. [[CrossRef](#)]
69. Tang, C.-W.; Wang, C.-B.; Chien, S.-H. Characterization of cobalt oxides studied by FT-IR, Raman, TPR and TG-MS. *Termochimica Acta* **2008**, *473*, 68–73. [[CrossRef](#)]
70. Eurov, D.A.; Rostovshchikova, T.N.; Shilina, M.I.; Kirilenko, D.A.; Tomkovich, M.V.; Yagovkina, M.A.; Udalova, O.V.; Kaplin, I.Y.; Ivanin, I.A.; Kurdyukov, D.A. Cobalt oxide decorated porous silica particles: Structure and activity relationship in the catalytic oxidation of carbon monoxide. *Appl. Surf. Sci.* **2022**, *579*, 152121. [[CrossRef](#)]
71. Wang, X.; Wang, X.; Yu, H.; Wang, X. The functions of Pt located at different positions of HZSM-5 in H₂-SCR. *Chem. Eng. J.* **2019**, *355*, 470–477. [[CrossRef](#)]
72. Gao, M.; Gong, Z.; Weng, X.; Shang, W.; Chai, Y.; Dai, W.; Wu, G.; Guan, N.; Li, L. Methane combustion over palladium catalyst within the confined space of MFI zeolite. *Chin. J. Catal.* **2021**, *42*, 1689–1699. [[CrossRef](#)]
73. Biesinger, M.C.; Payne, B.P.; Grosvenor, A.P.; Lau, L.W.M.; Gerson, A.R.; Smart, R.S.C. Resolving surface chemical states in XPS analysis of first row transition metals, oxides and hydroxides: Cr, Mn, Fe, Co and Ni. *Appl. Surf. Sci.* **2011**, *257*, 2717–2730. [[CrossRef](#)]
74. Lukashuk, L.; Föttinger, K.; Kolar, E.; Rameshan, C.; Teschner, D.; Havecker, M.; Knop-Gericke, A.; Yigit, N.; Li, H.; McDermott, E.; et al. Operando XAS and NAP-XPS studies of preferential CO oxidation on Co₃O₄ and CeO₂-Co₃O₄ catalysts. *J. Catal.* **2016**, *344*, 1–15. [[CrossRef](#)]
75. Morfin, F.; Nguyen, T.-S.; Rousset, J.-L.; Piccolo, L. Synergy between hydrogen and ceria in Pt-catalyzed CO oxidation: An investigation on Pt-CeO₂ catalysts synthesized by solution combustion. *Appl. Catal. B Environ.* **2016**, *197*, 2–13. [[CrossRef](#)]
76. Jiang, B.; Huang, M.; Cai, D.; Tan, K.B.; Zhan, G. Fabrication of Pt/Co₃O₄ nanocatalysts based on pollen template for low-temperature CO oxidation. *Cat. Commun.* **2023**, *174*, 106597. [[CrossRef](#)]
77. Li, C.; Ke, C.; Han, R.; Fan, G.; Yang, L.; Li, F. The remarkable promotion of in situ formed Pt-cobalt oxide interfacial sites on the carbonyl reduction to allylic alcohols. *Molec. Catal.* **2018**, *455*, 78–87. [[CrossRef](#)]

Disclaimer/Publisher's Note: The statements, opinions and data contained in all publications are solely those of the individual author(s) and contributor(s) and not of MDPI and/or the editor(s). MDPI and/or the editor(s) disclaim responsibility for any injury to people or property resulting from any ideas, methods, instructions or products referred to in the content.